A Robust LQG Servo Control Strategy of Shunt-Active Power Filter for Power Quality Enhancement

Rakhee Panigrahi, Bidyadhar Subudhi, *Senior Member, IEEE*, and Prafulla Chandra Panda, *Senior Member, IEEE*

***Abstract*—This paper proposes a linear quadratic Gaussian (LQG) servo controller for the current control of shunt-active power filter (SAPF) operating under balanced and unbalanced supply voltages. This LQG controller is comprised of a LQ regulator and a Kalman filter (KF) that minimizes the error between the output currents and their variations. A feedback compensator is used in LQG servo controller that benefits an SAPF system by increasing tracking error reduction, gain stability, reducing amplitude distortion and sensitivity to external disturbances. A KF-based new reference current generation scheme is developed here to resolve the difficulty of tuning gains of a proportional integral controller and for avoiding the use of voltage sensors making it cost effective. Consequently, this reference scheme has self-capability of dc-link voltage regulation by adaptively estimating the peak value of source reference current with changing load conditions. The control algorithm is embedded in SAPF using a MATLAB/Simulink software environment. The effectiveness of the proposed LQG Servo$_{\mathrm{KF}}$ algorithm is evaluated through comparison with an existing LQR$_{\mathrm{KF}}$ algorithm and then validated with experimental studies pursued using a dSPACE1104 computing platform. From the obtained experimental and simulation results, it is observed that the proposed control strategy exhibits superior performance in terms of robustness improvement and current harmonics mitigation under steady-state and dynamic load conditions, thus making it more effective for practical applications.**

***Index Terms*—Feedback compensator, Kalman filter (KF), linear quadratic Gaussian (LQG), measurement noise, reference current, robustness.**

I. Introduction

ELECTRICAL power quality [1], [2], [3] has been a growing concern because of the proliferation of the nonlinear loads, which causes significant increase of line losses, instability, and voltage distortion. With injection of harmonic current into the system, these nonlinear loads additionally cause low power factor. The resulting unbalanced current adversely affects every component in the power system and equipment. This results in poor power factor, increased losses, excessive neutral currents, and reduction in overall efficiency. Although load compensation using passive filters is simple to design and operate, it has drawbacks such as resonance, detuning, and overloading. The aforesaid issues can be effectively mitigated by employing a shunt-active power filter (SAPF).

Various control schemes have been applied in SAPF [4], [5] under both balanced and unbalanced loading conditions. However, these control strategies have not considered some important aspects of power system perturbations such as supply unbalance, variations in the SAPF as well as load parameters and grid perturbations such as measurement noise and voltage distortion. A linear quadratic control combined with an integral control has been employed to control a three-phase three-wire SAPF to achieve unity power factor at PCC of a heavily distorted and unbalanced load currents [6]. This control uses the full state vector available for feedback, but this is unrealistic as there is always a measurement noise. An optimal control theory [7] supported LQR and Kalman filter (KF) was proposed considering measurement noise, load currents, and grid voltage transients. However PCC voltage has not been considered as a disturbance in the SAPF model. LQR law is based on the availability of the complete state vector, which may not be completely measurable in most of the real-world situations. To overcome this, a LQG servo controller was proposed for voltage-source converter (VSC) connected to the grid [8], where KF was employed to estimate the state vector. In this case, power system perturbations have not been taken into consideration and also the presence of a time delay at the reference tracking point gives rise to a slow response of the overall system. Thus, tracking error is not reduced effectively and stability of the system is minimally improved. However, a fast response without any tracking error delay is indispensable for an SAPF system so that efficient current harmonics compensation can be achieved under aforementioned perturbations. To resolve the previous issues, in this paper, a modification of aforementioned LQG servo controller has been performed by employing a suitable feedback compensator having gain of $-(1/2)$, which has the capability of fast increasing tracking error reduction of the SAPF system by rejecting all types of perturbations raised in source and load areas. The idea behind this feedback compensator is to achieve gain stability, perfect tracking, and less current harmonics distortion.

Another important aspect of SAPF is the reference current generation, which ensures capacitor voltage regulation [9] under all types perturbations occurred in source and load sides and this voltage regulation is achieved by adjusting a small amount of real power flowing through shunt inverter into the dc-link capacitor. Further, this small amount of real power is adjusted by changing the peak value of the reference current. A PI controller [10] is normally used for determining this peak

Manuscript received January 24, 2015; revised May 21, 2015; accepted July 6, 2015. Date of publication July 14, 2015; date of current version November 30, 2015. Recommended for publication by Associate Editor Q.-C. Zhong.

The authors are with the Department of Electrical Engineering, National Institute of Technology, Rourkela 769008, India (e-mail: rpanigrahi99@gmail.com; bidyadhar@nitrkl.ac.in; pcpanda1948@gmail.com).

Color versions of one or more of the figures in this paper are available online at http://ieeexplore.ieee.org.

Digital Object Identifier 10.1109/TPEL.2015.2456155

value of reference current and its performance is satisfactory up to steady-state level. But when load changes, the peak value of reference current must be adjusted quickly to proportionally change the real power drawn from the source to keep satisfactory operation of SAPF. In this fashion, dc voltage regulation is directly dependent upon the peak value of reference source current. With aforementioned views, our proposed source reference current scheme is based upon estimation of the desired peak value of reference current adaptively employing KF, as a consequence capacitor voltage regulation is very fast with consideration of power system perturbations arisen in load as well as source sides.

It is not possible to supply quality power to the special equipment, e.g., programmable logic controller, distributed control system, converters in ac drives through conventional control schemes [6]–[8], [11] employed in SAPF. This results in malfunctioning of the above type of equipment, which need pure power at all moments with fast changing disturbances occurred in the power system. Hence, a fast and robust control action is necessary to supply pure and distortion less power to above equipment with all perturbations taken into account. In view of aforementioned issues, we focus on the development of robust LQG servo controller with a faster reference estimation scheme in SAPF, which permits all perturbations such as PCC voltage distortion, measurement noise, parametric variations of load, capacitor voltage and filter impedance, tracking error variations and supply voltage unbalance so that compensation capability of the overall SAPF system can be enhanced.

This paper is organized as follows. In Section II, the configuration of SAPF model along with the hardware description is presented. Section III briefly explains the proposed reference generation scheme together with proposed LQG servo controller strategy used in SAPF. The results obtained from simulation studies using MATLAB and hardware implementations are presented and discussed for various cases of power system perturbations in Section IV. Finally, the conclusion is presented in Section V.

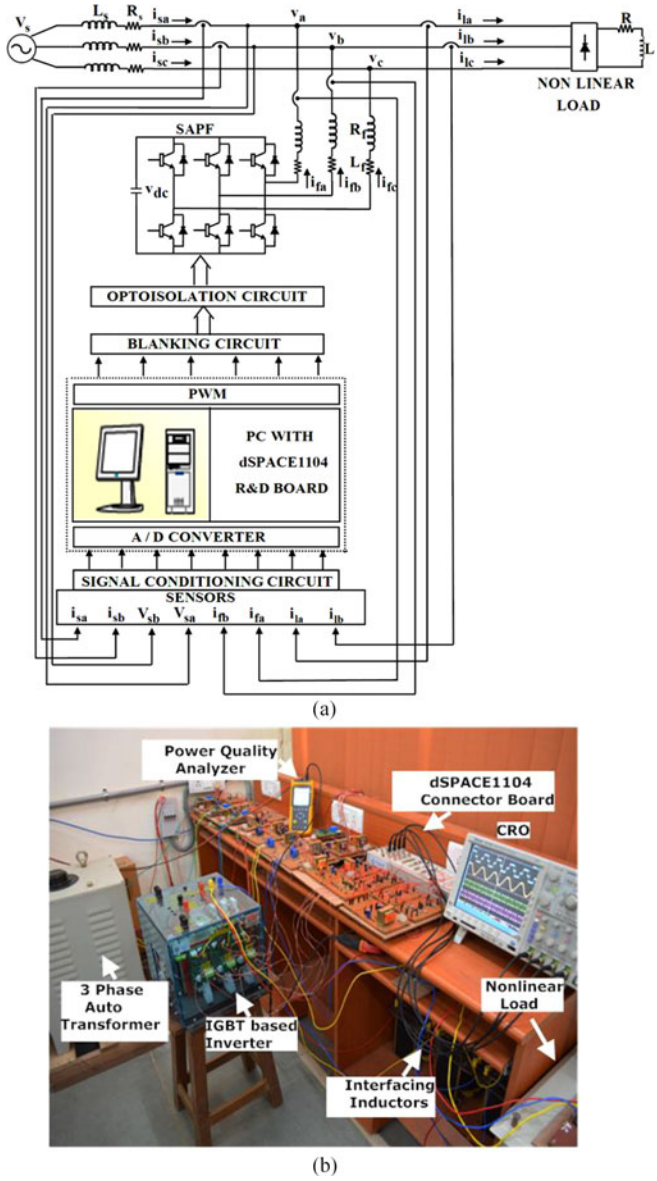

Fig. 1. Hardware details. (a) Block diagram of the control and power circuit of SAPF. (b) Experimental Setup.

II. Hardware Description of SAPF Model

The basic topology of a prototype SAPF developed in the laboratory prototype is presented in Fig. 1(a). This topology is composed of a voltage-source inverter connected to PCC through filter impedances (R_F, L_F). A nonlinear load comprising of a three-phase diode bridge rectifier with *RL* load is considered. The control of SAPF is achieved by LQG servo controller-based algorithm implemented with dSPACE1104. First, the controller is implemented using Simulink/MATLAB. The real-time workshop is used to generate C code for real-time applications. The interface between Simulink/MATLAB and dSPACE1104 permits running the control algorithm. The basic control structure and its mathematical equations are presented in Section III. The switching signals generated from the slave DSP (TMS320F240) are fed to blanking circuit (integrated circuit of SN74LS123) and opto-isolation circuit (high speed optocouplers ICHCPL2601). For implementation, the control algorithm is run at a fixed step size of 78.125 μs and hence, the maximum switching frequency of VSC of SAPF is fixed at 12.8 kHz. The design specifications and circuit parameters in laboratory prototype are given in Table I.

III. Development of the Control System

We present the control algorithm in the development of SAPF in two distinct steps namely reference generation and current controller implementation, which are described subsequently next.

A. Proposed Reference Current Generation Scheme

When load parameter varies, average voltage across the dc-link capacitor deviates from its reference value and the real power supplied by the source is not enough to supply the load demand. The SAPF cannot immediately respond to the load

TABLE I
SYSTEM PARAMETERS USED FOR SIMULATION AND EXPERIMENT

System parameter	Supply voltage RMS line–line (V_s) = 100 V
	Supply impedance (R_s = 0.1 Ω and L_s = 0.5 mH)
	Supply frequency (f) = 50 Hz
Load	Nonlinear load: three-phase diode bridge rectifier with resistive load of impedance (R = 20 Ω and L = 10 mH) (base case)
SAPF	DC-link capacitor (C) = 2350 μF;
	Reference DC-link voltage (v^*_{dc}) = 220 V;
	Filter impedance (R_f = 0.05 Ω and L_f = 2.5 mH)
	Switching frequency (f_{sw}) = 12.5 kHz
	Sampling frequency (f_s) = 25 kHz
PI controller	$K_p = 0.32, K_i = 1$

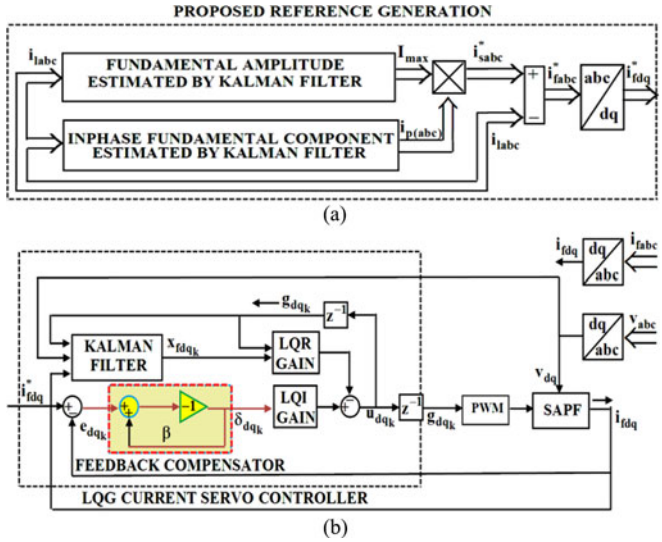

Fig. 2. Proposed control structure. (a) Proposed reference generation scheme. (b) Proposed LQG servo current controller strategy.

change since it takes a longer interval to calculate a new reference current. This drawback is overcome by the proposed reference scheme with a fast and adaptive estimation of peak value of source reference current, which has the capability of delivering real power equivalent to conduction and switching losses occurred during capacitor voltage deviation. As a result, it is expected that our proposed reference generation scheme can overcome the demerits of PI control and makes the dc-link capacitor voltage steady at the set point. This reference estimation approach has merit in avoidance of voltage sensors, tuning problems, and synchronization circuits needed for hardware; hence, it becomes cost effective.

The proposed scheme is based on source reference generation principle and the reference compensating currents $i^*_{f\mathrm{abc}}$ for three phases a, b, and c are generated by subtracting the source references i^*_{sabc} from the load currents $i_{l\mathrm{abc}}$ as shown in Fig. 2(a). Source reference current generation is implemented by the modulation of the estimated peak value of source current $(I_{\max})$ with the estimated in phase fundamental components $(i_{p(\mathrm{abc})})$ of load currents in per unit value, equations of which are provided next

$$i^*_{\mathrm{sabc}} = I_{\max} \times i_{p(\mathrm{abc})} \tag{1}$$

$$i^*_{f\mathrm{abc}} = i_{l\mathrm{abc}} - i^*_{\mathrm{sabc}}. \tag{2}$$

For an accurate estimation of reference current, the unit template $i_{p(\mathrm{abc})}$ must be undistorted and this condition is met by the Kalman filtering estimation algorithm.

1) Formulation of the KF Algorithm for Reference Current Generation: A linear signal z_k of single sinusoid is represented by

$$z_k = a_1 \sin(k\omega_1 T_s + \phi_1) \quad k = 1, \ldots, N \tag{3a}$$

$$\omega_1 = 2\pi f_1. \tag{3b}$$

In (3), T_s denotes the sampling time, parameters a_1 and f_1 are the fundamental amplitude and frequency, respectively, with initial phase ϕ_1. The signal z_{k+1} can be expressed as

$$z_{k+1} = x_{1_{k+1}} = x_{1_k} \cos(k\omega_1 T_s) + x_{2_k} \sin(k\omega_1 T_s). \tag{4}$$

Further

$$x_{2_{k+1}} = -x_{1_k} \sin(k\omega_1 T_s) + x_{2_k} \cos(k\omega_1 T_s) \tag{5}$$

where x_{2_k} is known as the in quadrature component and is orthogonal to x_{1_k} and they are represented by

$$x_{1_k} = a_1 \sin(k\omega_1 T_s + \phi_1) \tag{6a}$$

$$x_{2_k} = a_1 \cos(k\omega_1 T_s + \phi_1). \tag{6b}$$

To model amplitude or phase variations of the signal, a perturbation vector $\begin{bmatrix}\gamma_1 & \gamma_2\end{bmatrix}^T_k$ in the system states is considered with the state space representation as

$$x_{k+1} = \Phi_k x_k + w_k \tag{7}$$

$$y_k = H_k x_k + v_k \tag{8}$$

where w_k and v_k are the process and measurement noises, respectively, and the state transition matrix Φ_k and the observed value H_k are given as follows:

$$\Phi_k = \begin{bmatrix} \cos(\omega_1 T_s) & \sin(\omega_1 T_s) \\ -\sin(\omega_1 T_s) & \cos(\omega_1 T_s) \end{bmatrix} \tag{9}$$

$$H_k = [1 \quad 0]. \tag{10}$$

Denoting the estimate of x_{k+1} as $\hat{x}_{k+1|k}$, the sequential recursive computation steps for fundamental component identification are given by

$$\hat{x}_{k+1|k} = \Phi_k \hat{x}_{k|k-1} + K_k(y_k - H_k \hat{x}_{k|k-1}) \tag{11}$$

where

$$K_k = \Phi_k P_{k|k-1} H_k^T \left(H_k P_{k|k-1} H_k^T + R_{m_k}\right)^{-1} \tag{12}$$

is the Kalman gain and the error covariance matrix is given as follows:

$$P_{k+1|k} = \Phi_k P_{k|k-1} \Phi_k^T - K_k H_k P_{k|k-1} \Phi_k^T + Q_{m_k}. \tag{13}$$

Q_{m_k} and R_{m_k} are the process and measurement error covariance matrices, respectively

$$P_{k+1|k} = E\{(x_{k+1} - \hat{x}_{k+1|k})(x_{k+1} - \hat{x}_{k+1|k})^T\} \quad (14)$$

$$Q_{m_k} = E\{w_k w_k^T\} \quad (15)$$

$$R_{m_k} = E\{v_k v_k^T\}. \quad (16)$$

Based on the previous estimates ($\hat{x}_{1_{k|}}$ and $\hat{x}_{2_{k|}}$), the fundamental component's magnitude [12] is calculated as follows:

$$I_{\max} = \sqrt{\hat{x}_{1k}^2 + \hat{x}_{2k}^2}. \quad (17)$$

The in-phase fundamental component with per unit value $(i_{p(\mathrm{abc})})$can be expressed as

$$i_{p(\mathrm{abc})} = \sin(k\omega_1 T_s + \phi_1) = \frac{\hat{x}_{1_{k|}}}{I_{\max}}. \quad (18)$$

B. Proposed LQG Servo Current Controller

In the proposed LQG Servo controller, we consider a tradeoff but regulation/tracking performance and the control effort considering both process disturbances and measurement noise. We present next the design of our proposed LQG servo controller.

1) Design of the Proposed Feedback Compensator: The proposed feedback compensator plays a significant role in achieving gain stability, perfect reference tracking, less current harmonics distortion as well as improved bandwidth. Referring Fig. 2(b), the output of feedback compensator is expressed by the following equation:

$$\delta_{\mathrm{dq}_k} = e_{\mathrm{dq}_k} \times \beta \quad (19)$$

where β is the gain of feedback compensator and the corresponding gain value is determined as $(-1/2)$. e_{dq_k} is the tracking error of SAPF system and can be represented as

$$e_{\mathrm{dq}_k} = i^*_{f\mathrm{dq}_k} - i_{f\mathrm{dq}_k} \quad (20)$$

where $i_{f\mathrm{dq}}$ is the dq transformation of compensating current $i_{f\mathrm{abc}}$.

2) Construction of Kalman State Estimator: KF is used for measurement of harmonics [13], detection of grid perturbations [14], and estimation of fundamental component as well as system variables [15]. For linear systems contaminated with additive noise, KF is found to be an optimum estimator. In this paper, we need Kalman state estimator for LQG servo control because we cannot implement LQ optimal state feedback without full state measurement.

For implementation of the KF, one inherent computational delay is considered within the switch input u_{dq} to the SAPF system due to finite computation time and PCC voltage v_{dq} also acts as an input to the estimator. The linear discrete-time system in dq frame can be represented as

$$\begin{aligned} x_{f\mathrm{dq}_{k+1}} &= G_f x_{\mathrm{fdq}_k} + S_f u_{f\mathrm{dq}_k} + w_{f_k} \\ \mathrm{y}_{f\mathrm{dq}_k} &= C_f x_{f\mathrm{dq}_k} + v_{f_k} \end{aligned} \quad (21)$$

where w_{f_k} and v_{f_k} are modeled as white noise and the associated noise covariance matrices are given by W_f and V_f.

Further

$$\begin{aligned} x_{f\mathrm{dq}_k} &= \begin{bmatrix} i_{f\mathrm{d}_k} & i_{f\mathrm{q}_k} \end{bmatrix}^T \\ u_{f\mathrm{dq}_k} &= \begin{bmatrix} g_{\mathrm{dq}_k} & v_{\mathrm{dq}_k} \end{bmatrix}^T \end{aligned} \quad (22)$$

where

$$\begin{aligned} g_{\mathrm{dq}_k} &= u_{\mathrm{dq}_{k-1}} \\ G_f &= L^{-1}\{(sI - A)^{-1}\}|_{t=T_s} \end{aligned} \quad (23)$$

where

$$A = \begin{bmatrix} -\dfrac{R_f}{L_f} & \omega \\ -\omega & -\dfrac{R_f}{L_f} \end{bmatrix}$$

$$S_f = \begin{bmatrix} A^{-1}\left(e^{AT_s} - I\right)B_1 & A^{-1}\left(e^{AT_s} - I\right)B_2 \end{bmatrix} \quad (24)$$

where

$$B_1 = \begin{bmatrix} -\dfrac{R_f}{L_f} & \omega \\ -\omega & -\dfrac{R_f}{L_f} \end{bmatrix},\ B_2 = \begin{bmatrix} \dfrac{v_{dc}}{L_f} & 0 \\ 0 & \dfrac{v_{dc}}{L_f} \end{bmatrix}$$

$$C_f = C \quad (25)$$

where

$$C = \begin{bmatrix} 1 & 0 \\ 0 & 1 \end{bmatrix}. \quad (26)$$

The values of matrices A, B_1, B_2, and C prescribed in (24)–(26) are associated with the continuous state space model of SAPF [7].

The state estimation by KF is formulated in two steps [16] namely predictive and update. In the predictive step, $\hat{x}_{fdq_{k+1|k}}$ is determined from $\hat{x}_{fdq_{k|k}}$

$$P_{f_{k+1|k}} = G_f P_{\mathrm{f}_{k-1}} G_f^T + W_f \quad (27)$$

$$\hat{x}_{f\mathrm{dq}_{k+1|k}} = G_f \hat{x}_{f\mathrm{dq}_k} + G_f u_{f\mathrm{dq}_k}. \quad (28)$$

After measuring the output $y_{f\mathrm{dq}_k}$, the update step corrects the prior estimate-covariance pair $(\hat{x}_{f\mathrm{dq}_{k+1|k}}, P_{f_{k+1|k}})$ giving a posterior estimate-covariance pair $(\hat{x}_{f\mathrm{dq}_{k+1|k+1}}, P_{f_{k+1|k+1}})$. The update equations are represented as follows:

$$P_{f_{k+1|k+1}} = \left(\left(P_{f_{k+1|k}}\right)^{-1} + C_f V_f^{-1} C_f\right)^{-1} \quad (29)$$

$$\hat{x}_{f\mathrm{dq}_{k+1|k+1}} = \hat{x}_{f\mathrm{dq}_{k+1|k}} - P_{f_{k+1}} C_f^T V_f^{-1} \left(C_f \hat{x}_{f\mathrm{dq}_{k+1|k}} - y_{f\mathrm{dq}_k}\right). \quad (30)$$

3) Design of Optimal State Feedback Controller: For full state feedback control design, LQR design seeks to minimize the total transfer of energy from system input to output. The associated Riccati equation solution provides the optimal state feedback controller (K_{LQR}) that can minimize the cost function of the closed-loop system given as follows:

$$J = \frac{1}{2}\sum_{k=0}^{\infty}\{x_{f\mathrm{dq}_k}^T Q_L x_{f\mathrm{dq}_k} + u_{\mathrm{dq}_k}^T R_L u_{\mathrm{dq}_k}\} \quad (31)$$

where Q_L is a positive semi-definite matrix (state weighting matrix) and R_L is a positive-definite matrix (control weighting matrix). The entries of matrices Q_L and R_L are chosen such that the fastest dynamic response in the SAPF system can be achieved.

4) Formulation of the Proposed LQG Servo Controller: The proposed LQG servo controller ensures that the filter output current of SAPF ($i_{f\mathrm{dq}}$) tracks the reference command ($i^*_{f\mathrm{dq}}$) while rejecting process disturbances and measurement noise. The servo controller is the combination of optimal Kalman estimator and optimal state feedback controller and both designs are solved separately, based on the "separation principle."

The extended state space model of the proposed LQG servo controller equations according to Fig. 2(b) is given next

$$x_{\mathrm{servo}_{k+1}} = A_{\mathrm{servo}} x_{\mathrm{servo}_k} + B_{\mathrm{servo}} u_{\mathrm{dq}_k} \tag{32}$$

$$y_{\mathrm{servo}_k} = C_{\mathrm{servo}} x_{\mathrm{servo}_k} \tag{33}$$

$$u_{\mathrm{dq}_k} = -K_m x_{\mathrm{servo}_k} \tag{34}$$

where

$$x_{\mathrm{servo}_k} = \begin{bmatrix} i_{f\mathrm{d}_k} & i_{f\mathrm{q}_k} & g_{\mathrm{d}_k} & g_{\mathrm{q}_k} & \delta_{\mathrm{d}_k} & \delta_{\mathrm{q}_k} \end{bmatrix}^T \tag{35}$$

$$A_{\mathrm{servo}} = \begin{bmatrix} A_L & \vdots & 0 \\ \cdots & \vdots & \cdots \\ -C_L A_L & \vdots & 1 \end{bmatrix} \tag{36}$$

$$A_L = \begin{bmatrix} G_f & \vdots & S_f \\ \cdots & \vdots & \cdots \\ 0 & \vdots & 0 \end{bmatrix},\ C_L = \begin{bmatrix} 1 & 0 & 0 & 0 \\ 0 & 1 & 0 & 0 \end{bmatrix}$$

$$B_{\mathrm{servo}} = \begin{bmatrix} B_L \\ \cdots \\ -C_L B_L \end{bmatrix},\ B_L = \begin{bmatrix} 0 & 0 & 1 & 1 \end{bmatrix}^T \tag{37}$$

$$C_{\mathrm{servo}} = \begin{bmatrix} C_L & \vdots & 0 \end{bmatrix} \tag{38}$$

$$K_m = \begin{bmatrix} K_{\mathrm{LQR}} & \vdots & -K_{\mathrm{LQI}} \end{bmatrix}. \tag{39}$$

K_{LQI} and K_{LQR} are the linear quadratic integrator and linear quadratic regulator gains of the proposed LQG Servo controller, respectively, and the values of previous gains can be achieved from the solutions of the state space model of LQG servo controller.

IV. Results and Discussions

A. Simulation Results

A simulation model for the three-phase SAPF with the same parameters shown in Table I has been developed using MATLAB-Simulink. A triangular carrier-based pulse width modulation method is employed for driving three-phase IGBT inverter.

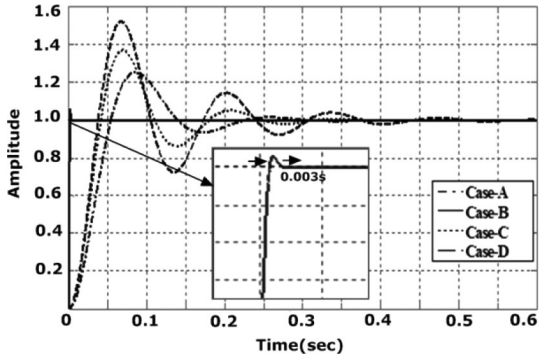

Fig. 3. Step response of the LQG servo control system with different matrices of Q_L.

For the LQR design, weighting matrices Q_L and R_L are used considering the conventional model of (21) extended to include different elements inside the state vector of (35). For simplicity, Q_L and R_L are chosen as $Q_L = diag\{q_1, q_2, q_3, q_4, q_5, q_6\}$ and $R_L = diag\{r_1, r_2\}$. Since the output currents $(i_{\mathrm{fd}}, i_{\mathrm{fq}})$ of SAPF appear to behave similarly, they should have accompanied with similar weights. Low or close to zero weighting may be placed on these states. But, for effective reactive power compensation through SAPF, the quadrature component (i_{fq}) should be little higher than in-phase component (i_{fd}), i.e., $q_1 \leq q_2$. Further, the states associated with the computational delays (g_d, g_q) are actually constrained given other states and hence they are assumed to be zero, i.e., $q_3 = q_4 = 0$. Taking into previous considerations and system symmetry, we have to choose $q_5 \leq q_6$ and also a fairly high weighting closer to one should be placed on the output of the feedback compensator in order to attain high bandwidth. We also need to consider the control effort limitation of u_d and u_q, which should be within $[-1, +1]$. Since R_L is considered to be more than Q_L to avoid large tracking error, we select $r_1 = r_2 = 1$. Taking into account aforementioned considerations, several choices for q_1, q_2, q_5 and q_6 have been used for analyzing the behavior of SAPF (Case-A: $q_1 = 0.000001, q_2 = 0.000003, q_5 = 0.75, q_6 = 0.79$; Case-B: $q_1 = 0.0031, q_2 = 0.0035, q_5 = 0.91, q_6 = 0.93$; Case-C: $q_1 = 0.043$, $q_2 = 0.045$, $q_5 = 0.94$, $q_6 = 0.96$; Case-D: $q_1 = 0.63$, $q_2 = 0.65$, $q_5 = 0.95$, $q_6 = 0.99$). It is seen by trial and error that with the choice of Case-B, the step response of the proposed LQG servo control system is quite satisfactory as depicted in Fig. 3, where settling time is found to be 3 ms. Thus, Q_L and R_L are expressed by

$$Q_L = \begin{bmatrix} 0.0031 & 0 & 0 & 0 & 0 & 0 \\ 0 & 0.0035 & 0 & 0 & 0 & 0 \\ 0 & 0 & 0 & 0 & 0 & 0 \\ 0 & 0 & 0 & 0 & 0 & 0 \\ 0 & 0 & 0 & 0 & 0.91 & 0 \\ 0 & 0 & 0 & 0 & 0 & 0.93 \end{bmatrix},$$

$$R_L = \begin{bmatrix} 1 & 0 \\ 0 & 1 \end{bmatrix}. \tag{40}$$

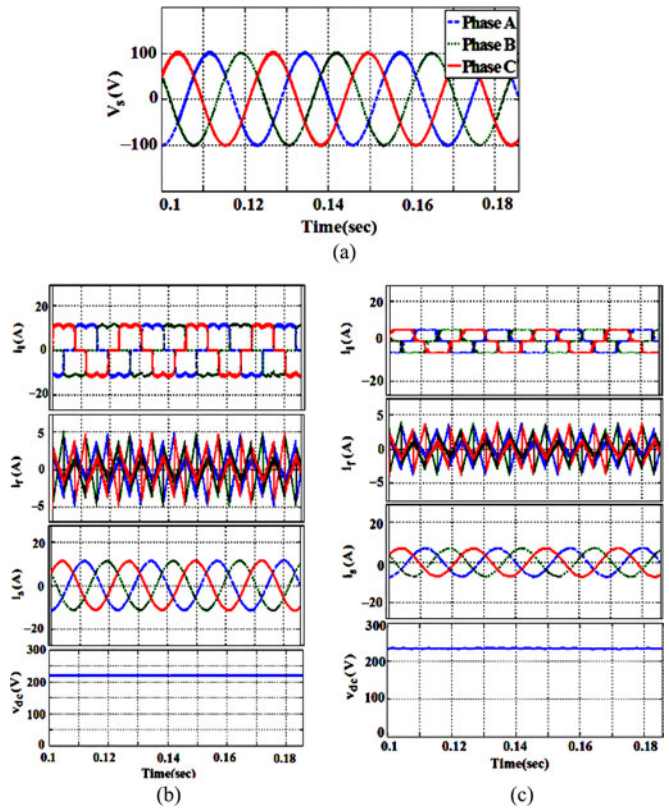

Fig. 4. Simulation results. (a) Waveforms of balanced supply voltages. (b) Response of the proposed SAPF in Case-1. (c) Response of the proposed SAPF in Case-2.

For KF design in reference current estimation, $Q_m = 0.01\ I_{22}A^2$ and $R_m = 20A^2$ were chosen initially to tune KF in simulation. Further, the weighting signal is minimized more with increase of weighting parameter. Hence, the simulation process is continued by increasing the aforementioned covariance values until an optimality of KF can be enriched. After several iteration processes, Q_m and R_m are set to $0.05I_{22}A^2$ and $200A^2$. Similarly, W_f and V_f are set to $0.1I_{22}A^2$ and $300A^2$, respectively, for KF implementation in LQG servo controller.

The simulation results obtained with the proposed SAPF are shown in Fig. 4 considering two Cases (Case-1: steady-state load condition; Case-2: load impedances are increased by 50%). The supply voltage waveforms are shown in Fig. 4(a). Fig. 4(b) presents the steady-state performance of SAPF when the load impedances are kept at the base value (100%). The load current, compensating current, source current, and the capacitor voltage are shown for three phases in top to bottom order. The compensated source currents are found to be sinusoidal.

Similar results are found for Case-2 as seen in the respective graphs shown in Fig. 4(c). The robustness of proposed SAPF is analyzed here. The harmonics distortion results of the source current for phase "a" before compensation and after compensation with proposed SAPF in both cases are given in Table II. In Case-1, the source current total harmonics distortion (THD) is reduced from 25.67% to 3.18%. When load impedance is increased by 50%, the THD is reduced from 21.44% to 2.59%

TABLE II
HARMONICS COMPENSATION EFFECT OF THE PROPOSED $\mathrm{LQGServo_{KF}}$-BASED SAPF (SIMULATION)

Cases	THD% of phase-a source current		
	Before compensation THD (%)	After compensation THD (%)	HCR (%)
Case-1	25.67	3.18	12.38
Case-2	21.44	2.59	12.11

and also the harmonics compensation ratio (HCR) is differed by only 0.27%. Therefore, THDs of the source current are unaffected by the parametric variations of the load. This shows the robustness of the proposed SAPF under parametric variations of the load. The HCR factor is calculated as follows:

$$\mathrm{HCR} = \frac{\mathrm{THD\%\ After\ Compensation}}{\mathrm{THD\%\ Before\ Compensation}} \times 100\%. \qquad (41)$$

B. Experimental Results

The proposed control algorithm has been implemented in real time on the hardware setup developed in our Lab. A photograph of the experimental setup is shown in Fig. 1 (b). The efficacy of the proposed scheme is compared with the existing method ($\mathrm{LQR_{KF}}$) [7], where LQR is employed as current controller and KF for reference current generation in SAPF. The experimental studies for both steady state and dynamic conditions are performed and discussed in the following sections.

Case 1: Balanced supply voltages-steady-state load condition. The performance of the proposed SAPF is analyzed with the base case load impedance. A diode bridge rectifier with a resistive-inductive load is chosen as the test load to study the operation of SAPF for load compensation. The three-phase unit templates (u_a, u_b, u_c) estimated by KF are shown in Fig. 5(a). It is seen that unit templates are undistorted and sinusoidal. Fig. 5(b) and (c) show the load currents $(i_{\mathrm{la}}, i_{\mathrm{lb}}, i_{\mathrm{lc}})$ and compensating currents $(i_{\mathrm{fa}}, i_{\mathrm{fb}}, i_{\mathrm{fc}})$ in phases a, b, and c, respectively. The overall performance of the proposed $\mathrm{LQGServo_{KF}}$-based SAPF is shown in Fig. 5(d). The waveforms shown in this figure are phase-a source voltage, compensating current, source current, and dc-bus voltage. The source current is found to be almost sinusoidal. The reference tracking behavior of the compensating current for both the proposed and existing method is presented in Fig. 6(a) (i) and (ii), respectively. It is observed that a tracking delay of "1 ms" is arisen in existing one, whereas it is zero for the proposed method resulting toward an excellent tracking behavior of the $\mathrm{LQGServo_{KF}}$-based SAPF system. Further, the waveforms of the source current are shown with start-on condition for the proposed as well as existing method [see Fig. 6(b) (i) and (ii)]. The source currents in case of proposed approach are observed to be smooth and distortion less as compared to the existing method. The harmonic spectra are analyzed using a power quality analyzer and the recorded harmonic spectra for uncompensated as well as compensated phase "a" current are shown in Fig. 7. The THD in the load current is as high as 25.9%, but the THD in the source current has been

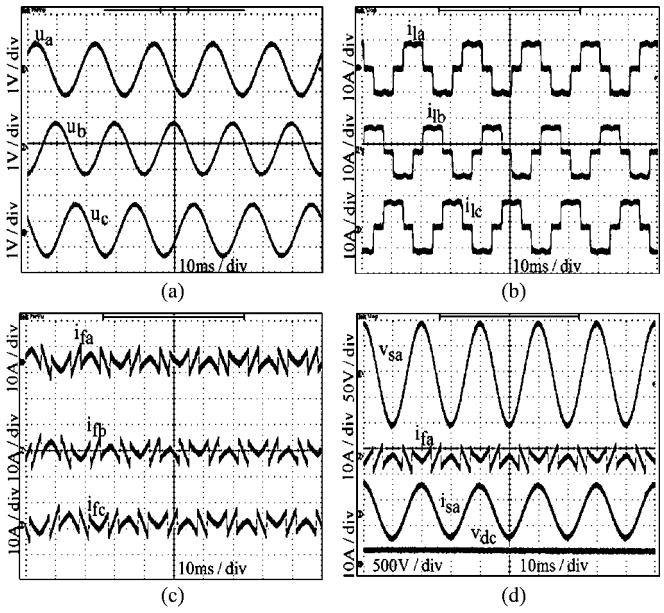

Fig. 5. Case-1: (a) unit voltage templates, (b) three-phase load currents, (c) three-phase compensating currents in the proposed method, and (d) phase-a quantities in the proposed method.

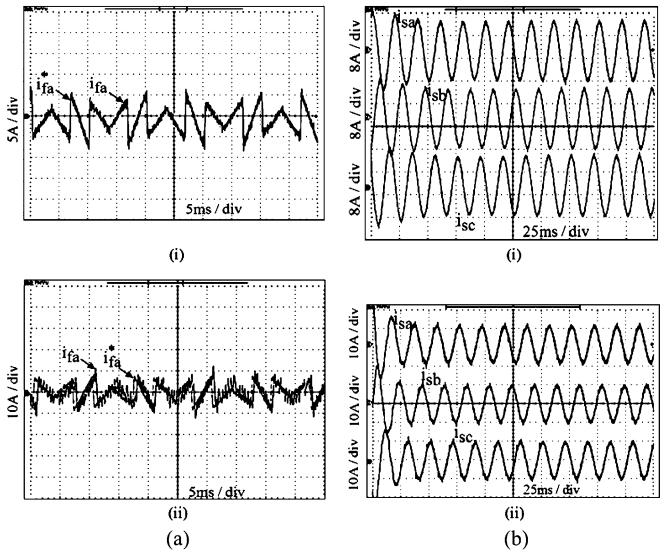

Fig. 6. Case-1: (a) waveform showing tracking behavior of compensating current and (b) waveforms of three-phase source currents (with start-on condition). (i) Proposed method. (ii) Existing method.

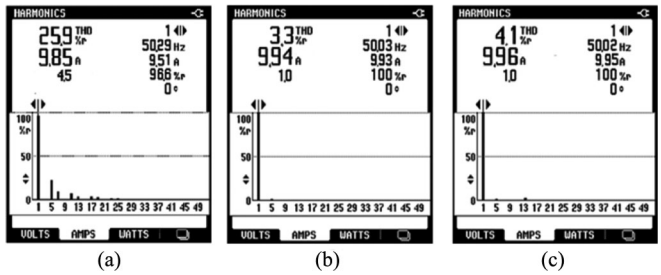

Fig. 7. Case-1: harmonic spectra of (a) phase-a load current, (b) phase-a source current in the proposed method, and (c) phase-a source current in existing method.

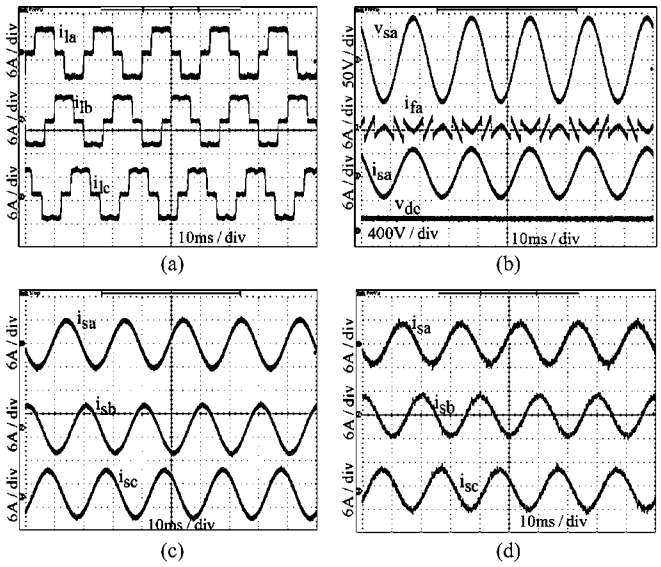

Fig. 8. Case-2: (a) three-phase load currents, (b) phase-a quantities in the proposed method, (c) three-phase source currents in the proposed method, and (d) three-phase source currents in existing method.

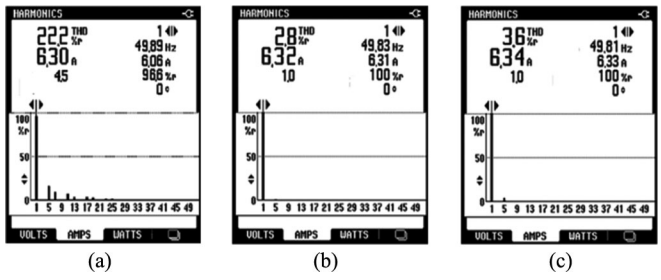

Fig. 9 Case-2: harmonics spectra of (a) phase-a load current, (b) phase-a source current in the proposed method, and (c) phase-a source current in existing method.

lowered to 3.3% and 4.1% in case of the proposed and existing method, respectively. Hence, it can be concluded that the proposed LQGServo$_{\mathrm{KF}}$-based SAPF provides better reduction in %THD as a requirement set by IEEE519 standard.

Case 2: Balanced supply voltages—load impedances are increased by 50%. In this case, the load impedances have been increased by 50% from the base case without alternating any other parameters of the system. Fig. 8(a) shows the three-phase load currents, where the amplitude is reduced by 4 A as compared to Case-1. Fig. 8(b) shows the compensation characteristics of the proposed SAPF. The source voltage is kept at 100 V and the dc-link voltage is maintained at 220 V. Fig. 8(c) shows the three-phase source currents which are all balanced (≈6.32 A) and sinusoidal in the proposed SAPF; however, distortions are observed in case of existing method as depicted in Fig. 8(d). The harmonic spectra for load and source current are specified in Fig. 9 employing aforementioned two methods. The THD of

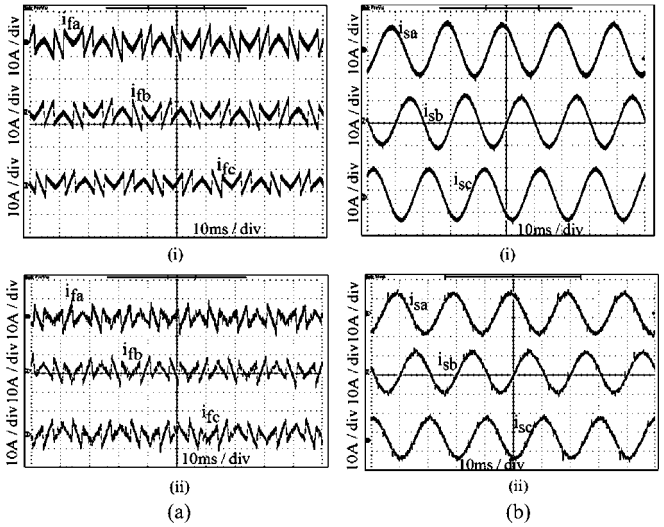

Fig. 10. Case-3: (a) three-phase compensating currents and (b) three-phase source currents. (i) Proposed method. (ii) Existing method.

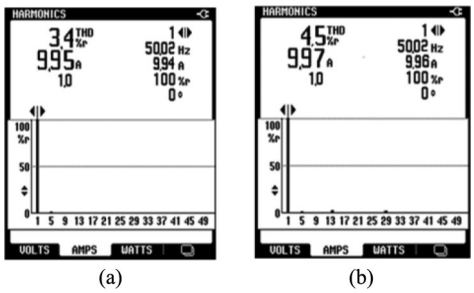

Fig. 11. Case-3: harmonics spectra of (a) phase-a source current in the proposed method and (b) phase-a source current in existing method.

the load current is reduced from 22.2% to an extent of 2.8% in case of the proposed method whereas it is reduced to 3.6% in case of existing method. It is observed that even under parametric variations of load, the proposed control scheme behaves better than the existing control strategy.

Case 3: Balanced supply voltages—changing SAPF parameters. In this case, the SAPF parameters are increased from $R_f = 0.05\,\Omega, L_f = 2.5\,\mathrm{mH}$ to $R_f = 0.5\,\Omega, L_f = 3\,\mathrm{mH}$. Under this condition, the performance of the proposed control algorithm is verified with existing technique through Figs. 10 and 11. It is seen that in case of the proposed approach the waveforms for compensating current and the source current are smooth and distortion less as compared to the existing $\mathrm{LQR}_{\mathrm{KF}}$ method. Hence, the effective harmonics compensation is more in case of the proposed $\mathrm{LQGServo}_{\mathrm{KF}}$ method. Also, the THD of phase-a source current after compensation is analyzed in Fig. 11, which shows the superiority of the proposed method (i.e., THD $= 3.4\%$) over existing method (i.e., THD $= 4.5\%$).

Case 4: Balanced supply voltages—dynamic load condition. The performance of the proposed SAPF, considering the balanced supply voltages, during a sudden load change condition is illustrated in Fig. 12(a). To create dynamic condition, the load is changed from $(R = 30\,\Omega, L = 15\,\mathrm{mH})$ to

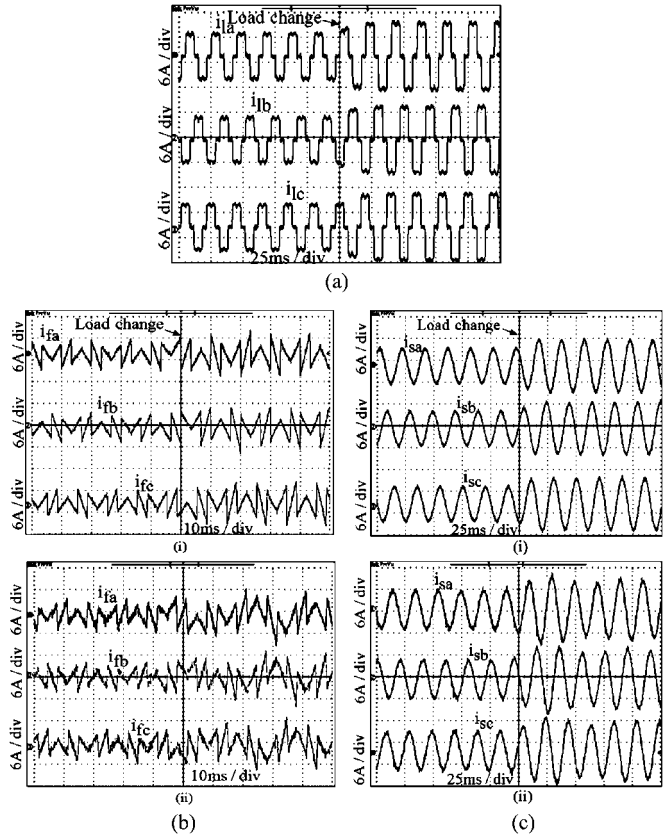

Fig. 12. Case-4: (a) three-phase load currents, (b) three-phase compensating currents, and (c) three-phase source currents. (i) Proposed method. (ii) Existing method.

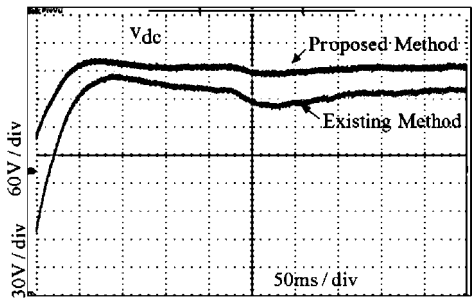

Fig. 13. Case -4: waveforms of capacitor voltages in the proposed and existing method.

$(R = 20\,\Omega, L = 10\,\mathrm{mH})$. As soon as the load is changed, the compensating current quickly responds to changes to compensate the harmonic currents in the load, as shown in Fig. 12(b). Also, the compensated source current profiles can be viewed from Fig. 12(c) for both existing and proposed techniques. As noticed, the SAPF system with proposed $\mathrm{LQGServo}_{\mathrm{KF}}$ approach achieves better compensation waveforms as compared to $\mathrm{LQR}_{\mathrm{KF}}$. Furthermore, the dc-link voltage in case of existing method settles to the reference value with a time delay of 0.1 s, while a delay of only 0.025 s is created for the proposed method as illustrated in Fig. 13. Fig. 14 shows that the supply current THD is effectively reduced from 26.8% to 3.5% and 4.9% in the proposed and existing method, respectively. Thus,

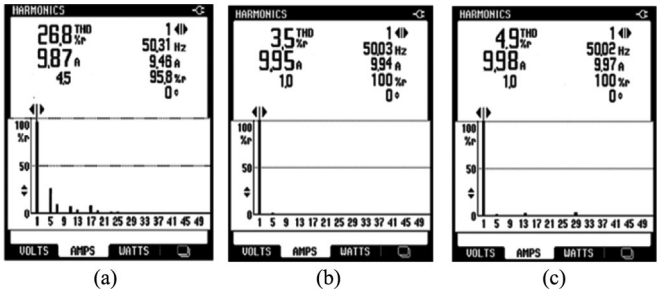

Fig. 14. Case-4: harmonics spectra of (a) phase-a load current, (b) phase-a source current in the proposed method, and (c) phase-a source current in existing method.

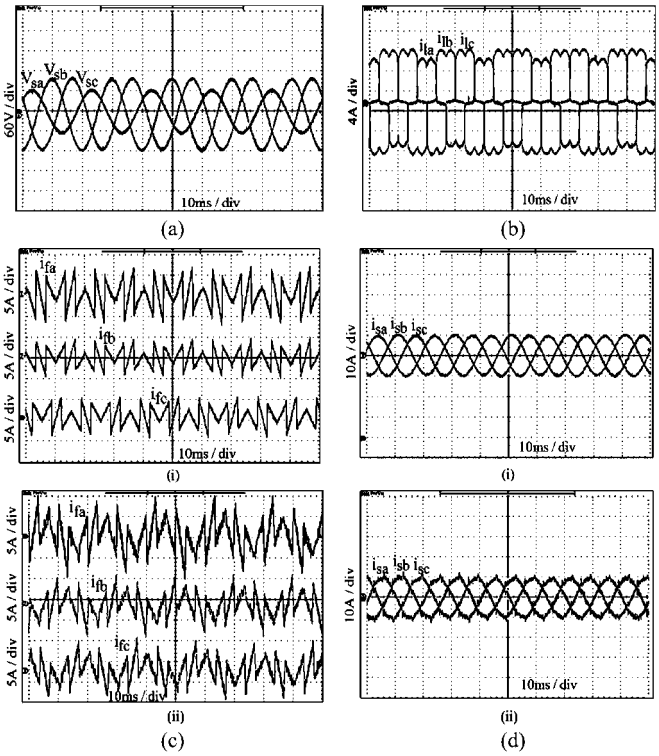

Fig. 15. Case-5: (a) three-phase supply voltages, (b) three-phase load currents, (c) three-phase compensating currents. (d) Three-phase source currents. (i) Proposed method. (ii) Existing method.

this dynamic condition demonstrates the true capability and enhanced performance of the proposed $\mathrm{LQGServo_{KF}}$ algorithm over $\mathrm{LQR_{KF}}$-based approach.

Case 5: Unbalanced supply voltages–steady-state load condition. In majority of previous cases, the supply voltage has usually been assumed to be sinusoidal and balanced, but this voltage condition is rare in practical networks. The unbalanced supply voltage condition in practical networks may adversely affect the control performance of the SAPF. To verify the effectiveness of the proposed control algorithm under such condition, experiments were carried out. The profiles for three-phase supply voltages and load currents are given in Fig. 15(a) and (b). To create unbalance, three sensors are required for three phases and phase-a voltage is reduced by 40 V as depicted in Fig. 15(a). As a result, phase-a compensating current is increased more to

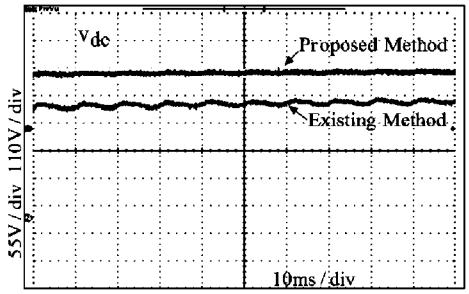

Fig. 16. Case-5: waveforms of capacitor voltages in the proposed and existing method.

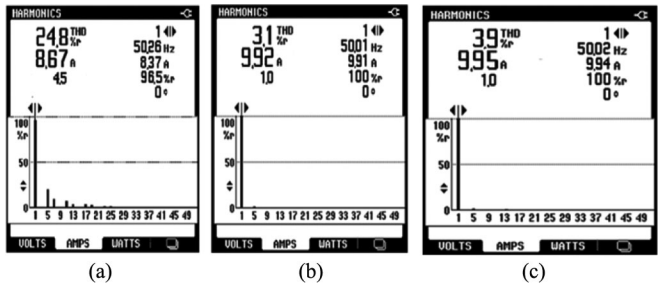

Fig. 17. Case-5: harmonics spectra of (a) phase-a load current, (b) phase-a source current in the proposed method, and (c) phase-a source current in existing method.

counteract the unbalance as shown in Fig. 15(c). However, the shapes of the compensating current waveforms are smoother in case of the proposed algorithm. As shown in Fig. 15(d), the harmonic compensation performance of the SAPF is not deteriorated at unbalanced supply voltage condition and the supply currents are balanced. But, a number of spikes are observed in case of existing method. Furthermore, the dc-link voltage, as shown in Fig. 16, is effectively regulated at the set reference value by employing the proposed $\mathrm{LQGServo_{KF}}$ method. From THD factor analysis for phase-a source current shown in Fig. 17, the proposed method has lower THD (i.e. 3.1%) as compared to existing $\mathrm{LQR_{KF}}$ (i.e., 3.9%), whereas the load current is distorted with a THD factor of 24.8%.

It is verified through experiments that the proposed $\mathrm{LQG\ Servo_{KF}}$-based SAPF has better steady-state performances as well as better dynamic responses as compared to existing approach. In addition, to evaluate the robustness performance of the existing $\mathrm{LQR_{KF}}$ controller and the proposed $\mathrm{LQGServo_{KF}}$ controller considering aforementioned five cases, HCR factors are calculated and summarized in Table III. The results in Table III demonstrate that in case of the proposed approach, HCR factors are maintained nearly the same (i.e., close to 13%) and these factors are unaffected by any perturbations raised in load or source sides, which makes the SAPF system more robust. In contrast, such robustness cannot be achieved by using existing control strategy, in which HCR factor is largely deviated (i.e., a deviation of 3%) in the presence of transient behavior of the load. Thus, the superiority of the proposed algorithm over existing $\mathrm{LQR_{KF}}$ is highlighted through all situations of power system perturbations.

TABLE III
HARMONICS COMPENSATION EFFECT OF THE PROPOSED AND EXISTING CONTROL STRATEGY IN SAPF (EXPERIMENTAL)

Cases	Methods used in SAPF	THD% of phase-a source current		
		Before compensation THD (%)	After compensation THD (%)	HCR (%)
Case 1	LQG Servo_{KF}	25.9	3.3	12.74
	LQR_{KF}	25.9	4.1	15.83
Case 2	LQG Servo_{KF}	22.2	2.8	12.61
	LQR_{KF}	22.2	3.6	16.21
Case 3	LQG Servo_{KF}	25.9	3.4	13.12
	LQR_{KF}	25.9	4.5	17.37
Case 4	LQG Servo_{KF}	26.8	3.5	13.05
	LQR_{KF}	26.8	4.9	18.28
Case 5	LQG Servo_{KF}	24.8	3.1	12.5
	LQR_{KF}	24.8	3.9	15.76

V. CONCLUSION

We presented a robust LQG servo controller design for an SAPF. The robustness of the proposed LQG servo controller strategy has been verified by analyzing the performance under steady state as well as dynamic condition of the power system. From the obtained simulation as well as experimental results, the proposed SAPF has been observed to provide efficient current harmonics mitigation, reference current tracking behavior, and reactive power compensation with dynamically changing load conditions (other LQR-based approaches are limited to steady-state conditions).

In the presence of an additive white Gaussian noise, switching noise, and distortion at PCC voltage, KF is found to be the best option involving both in reference generation and current controller realization of SAPF. The proposed reference scheme acts as a self-regulator of dc-link voltage escaping from external linear and nonlinear controller and hence an inexpensive control strategy can be implemented. Furthermore, the main feature of the LQG servo controller is the feedback compensator, which has effects of reducing tracking error distortion, noise and hence a perfect gain stability of the SAPF system is achieved.

REFERENCES

[1] Z. Zheng, Y. Huan, T. Shengqing, and Z. Rongxiang, "Objective-oriented power quality compensation of multifunctional grid-tied inverters and its application in microgrids," *IEEE Trans. Power Electron.*, vol. 30, no. 3, pp. 1255–1265, Mar. 2015.

[2] D. Divan, R. Moghe, and A. Prasai, "Power electronics at the grid edge: The key to unlocking value from the smart grid," *IEEE Power Electron. Mag.*, vol. 1, no. 4, pp. 16–22, Dec. 2014.

[3] M. Ali, E. Laboure, and F. Costa, "Integrated active filter for differential-mode noise suppression," *IEEE Trans. Power Electron.*, vol. 29, no. 3, pp. 1053–1057, Mar. 2014.

[4] R. L. A. Ribeiro, C. C. Azevedo, and R. M. Sousa, "A robust adaptive control strategy of active power filters for power-factor correction, harmonic compensation, and balancing of nonlinear loads," *IEEE Trans. Power Electron.*, vol. 27, no. 2, pp. 718–730, Feb. 2012.

[5] B. Singh and J. Solanki, "An implementation of an adaptive control algorithm for a three phase shunt active filter," *IEEE Trans. Ind. Electron.*, vol. 56, no. 8, pp. 2811–2820, Aug. 2009.

[6] B. Kedjar and K. Al-Haddad, "DSP-based implementation of an LQR with integral action for a three phase three wire shunt active power filter," *IEEE Trans. Ind. Electron.*, vol. 56, no. 8, pp. 2821–2828, Aug. 2009.

[7] M. Kanieski, R. Cardoso, H. Pinheiro, and H. A. Grundling, "Kalman filter based control system for power quality conditioning devices," *IEEE Trans. Ind. Electron.*, vol. 60, no. 11, pp. 5214–5227, Nov. 2013.

[8] F. Huerta, D. Pizarro, S. Cobreces, F. J. Rodriguez, C. Giron, and A. Rodriguez, "LQG servo controller for the current control of LCL grid connected voltage source converters," *IEEE Trans. Ind. Electron.*, vol. 59, no. 11, pp. 4272–4284, Nov. 2012.

[9] W. H. Choi, C. S. Lam, M. C. Wong, and Y. D. Han, "Analysis of dc-link voltage controls in three-phase four-wire hybrid active power filters," *IEEE Trans. Power Electron.*, vol. 28, no. 5, pp. 2180–2191, May 2013.

[10] J. F. Petit, G. Robles, and H. Amaris, "Current reference control for shunt active power filters under non sinusoidal voltage conditions," *IEEE Trans. Power Del.*, vol. 22, no. 4, pp. 2254–2261, Oct. 2007.

[11] S. Hu, Z. Zhang, Y. Li, L. Luo, Y. Cao, and C. Rehtanz, "A new half-bridge winding compensation-based power conditioning system for electric railway with LQRI," *IEEE Trans. Power Electron.*, vol. 29, no. 10, pp. 5242–5256, Oct. 2014.

[12] R. Cardoso, R. F. D. Camargo, H. Pinheiro, and H. A. Grunling, "Kalman filter based synchronization methods," *IET Gener., Transmiss. Distrib.*, vol. 2, no. 4, pp. 542–555, Jul. 2008.

[13] P. K. Ray and B. Subudhi, "Ensemble Kalman filtering algorithm applied to power system harmonics estimation," *IEEE Trans. Instrum. Meas.*, vol. 61, no. 12, pp. 3216–3224, Dec. 2012.

[14] N. Hoffmann and F. W. Fuchs, "Minimal invasive equivalent grid impedance estimation in inductive-resistive power networks using extended Kalman filter," *IEEE Trans. Power Electron.*, vol. 29, no. 2, pp. 631–641, Feb. 2014.

[15] R. Panigrahi, B. Subudhi, and P. C. Panda, "Model predictive-based shunt active power filter with a new reference current estimation strategy," *IET Power Electron.*, vol. 8, no. 2, pp. 221–233, Feb. 2015.

[16] B. Teixeira, "Kalman filters [ask the experts]," *IEEE Control Syst. Mag.*, vol. 28, no. 2, pp. 16–18, Apr. 2008.

Rakhee Panigrahi received the B.E. degree in electrical engineering from the University College of Engineering, Burla, Odisha, India, in 2002, and the M.Tech. degree in electrical engineering from the National Institute of Technology, Rourkela, India, in 2009, where she is currently working toward the Ph.D. degree in the Department of Electrical Engineering.

Her research is focused on estimation techniques with application to power quality.

Bidyadhar Subudhi (SM'08) received the Bachelor's degree in electrical engineering from the National Institute of Technology, Rourkela, India, in 1988, the Master of Technology in Control & Instrumentation from the Indian Institute of Technology, Delhi, India, in 1994, and the Ph.D. degree in control system engineering from the University of Sheffield, Sheffield, U.K., in 2003.

He is currently a Professor in the Department of Electrical Engineering, National Institute of Technology, Rourkela, India, and a Coordinator in the Centre of Excellence on Renewable Energy Systems. His research interests include system identification and adaptive control, estimation and filtering with application to power system and control of renewable energy systems.

Dr. Subudhi is a Fellow of the IET.

Prafulla Chandra Panda (SM'05) received the B.Sc., M.Sc., and Ph.D. degrees from Sambalpur University, Odisha, India, in 1971, 1974, and 1990, respectively, all in electrical engineering.

Since 1977, he has been with the National Institute of Technology, Rourkela, India, as a Professor in the Department of Electrical Engineering. At present, his research interests include power system dynamic stability analysis, power quality and high voltage dc transmission.